Adhesion GPCR Latrophilin 3 regulates synaptic function of cone photoreceptors in a trans-synaptic manner

Yuchen Wang[a], Yan Cao[a], Cassandra L. Hays[b], Thibaut Laboute[a], Thomas A. Ray[c], Debbie Guerrero-Given[d], Abhimanyu S. Ahuja[a], Dipak Patil[a], Olga Rivero[e], Naomi Kamasawa[d], Jeremy N. Kay[c], Wallace B. Thoreson[b], and Kirill A. Martemyanov[a,1]

[a]Department of Neuroscience, The Scripps Research Institute, Jupiter, FL 33458; [b]Truhlsen Eye Institute, Durham Research Center I, University of Nebraska Medical Center, Omaha, NE 68198-5840; [c]Department of Neurobiology and Ophthalmology, and Cell Biology, Duke University School of Medicine, Durham, NC 27710; [d]Electron Microscopy Core Facility, Max Planck Florida Institute, Jupiter, FL 33458; and [e]Division of Molecular Psychiatry, Center of Mental Health, University of Würzburg 97080 Würzburg, Germany

Edited by Alex L. Kolodkin, Johns Hopkins University, Baltimore, MD, and accepted by the Editorial Board September 23, 2021 (received for review April 8, 2021)

Cone photoreceptors mediate daylight vision in vertebrates. Changes in neurotransmitter release at cone synapses encode visual information and is subject to precise control by negative feedback from enigmatic horizontal cells. However, the mechanisms that orchestrate this modulation are poorly understood due to a virtually unknown landscape of molecular players. Here, we report a molecular player operating selectively at cone synapses that modulates effects of horizontal cells on synaptic release. Using an unbiased proteomic screen, we identified an adhesion GPCR Latrophilin3 (LPHN3) in horizontal cell dendrites that engages in transsynaptic control of cones. We detected and characterized a prominent splice isoform of LPHN3 that excludes a element with inhibitory influence on transsynaptic interactions. A gain-of-function mouse model specifically routing LPHN3 splicing to this isoform but not knockout of LPHN3 diminished $Ca_V1.4$ calcium channel activity profoundly disrupted synaptic release by cones and resulted in synaptic transmission deficits. These findings offer molecular insight into horizontal cell modulation on cone synaptic function and more broadly demonstrate the importance of alternative splicing in adhesion GPCRs for their physiological function.

retina | adhesion GPCR | synapses | horizontal cells | vision

Vision is a key sensory modality essential for the survival of most living organisms. In mammals, it is enabled by the retina: a neural structure composed of more than 60 distinct neurons each uniquely wired into the circuitry and with particular roles in image processing (1, 2). Vision begins with the detection of light by rod and cone photoreceptors. Rod photoreceptor cells are exquisitely sensitive to light and mediate vision at low light levels (3, 4). However, most vertebrates including humans rely on cone cells for daytime vision (5). Accordingly, cones have an extremely broad range of light sensitivity spanning 6 to 7 orders of magnitude (6), quickly adapting to changes in luminance and providing high spatial and temporal visual acuity (5, 7, 8). The molecular, cellular, and circuit mechanisms that allow cones to perform their tasks has been a subject of intense interest, providing groundbreaking discoveries that illuminate fundamental organizational principles that govern signal processing by neural circuits in general.

The capture and processing of photons by the phototransduction cascade of cones generates graded changes in membrane potential: hyperpolarizing to light and depolarizing with darkness (7). These voltage signals alter the ongoing rate of neurotransmitter glutamate release at the cone synapse to relay information about light and dark to the retinal circuitry (9). The molecular entity that mediates this transformation is the L-type voltage-gated Ca^{2+} channel, $Ca_V1.4$ (10–12). It is located at specialized active zones containing synaptic ribbons and couples light-driven changes in voltage to changes in local Ca^{2+} levels thereby regulating the vesicular fusion machinery (13, 14). The $Ca_V1.4$ channel forms a macromolecular complex with a number of synaptic molecules and thus plays a pivotal role in both the structural and functional organization of the presynaptic active zone of photoreceptors (15). Accordingly, changes in $Ca_V1.4$ function imposed by binding partners or environment have a tremendous impact on the synaptic communication of cone photoreceptors and vision (16–18).

Cones form synaptic contacts with three types of neurons. They synapse with postsynaptic ON- and OFF-type bipolar cells (BC) to relay visual information to the downstream neuronal circuitry (19, 20). Cones also contact lateral inhibitory neurons known as horizontal cells (HCs) that connect adjacent to BC dendrites, forming a tripartite synaptic triad (20). This elaborate synaptic arrangement of cones is a site of major influence on how visual information is processed contributing to unique cone physiology and adaptive capacity for daylight detection (21, 22).

The function of HCs and their physiological mechanisms are particularly intriguing. HCs powerfully modulate synaptic transmission at cone synapses (23). Light-evoked hyperpolarization

Significance

This study addresses a fundamental question in neuroscience: how do neurons functionally specify and diversify their synaptic connections? This question is particularly relevant in the visual system in which neurons handle a broad range of stimuli requiring synapses to adjust their gain accordingly. In this work, we describe how synapses of cone photoreceptors, which all vertebrate animals utilize for daylight vision, handle this task through an elegant transsynaptic mechanism involving a splice isoform of a cell-adhesion molecule, Latrophillin 3.

Author contributions: Y.W., J.N.K., W.B.T., and K.A.M. designed research; Y.W., Y.C., C.L.H., T.L., T.A.R., D.G.-G., A.S.A., D.P., and N.K. performed research; O.R. contributed new reagents/analytic tools; Y.W., Y.C., C.L.H., T.L., T.A.R., D.G.-G., A.S.A., D.P., N.K., J.N.K., W.B.T., and K.A.M. analyzed data; and Y.W., W.B.T., and K.A.M. wrote the paper.

The authors declare no competing interest.

This article is a PNAS Direct Submission. A.L.K. is a guest editor invited by the Editorial Board.

[1]To whom correspondence may be addressed. Email: kirill@scripps.edu.

This article contains supporting information online at http://www.pnas.org/lookup/suppl/doi:10.1073/pnas.2106694118/-/DCSupplemental.

Published November 3, 2021.

of HCs counteracts light-induced suppression of glutamate release from cone terminals, thereby providing strong negative feedback (23, 24). Because each HC contacts multiple cones, this negative influence on surrounding cones is a major mechanism for producing lateral inhibition, a classical feature of signal processing in the retina that enhances contrast and spatial resolution of vision (25). In addition, feedback from individual HC dendrites to specific cone terminals and ribbons can also act locally, fine-tuning synaptic output to local illumination gradients (26–29).

While the role of HCs from a circuit perspective is well understood, the mechanisms that they use to provide negative feedback are subject to debate and controversy. At least three different explanations have been provided: direct ephaptic effects (30, 31), changes in synaptic pH (28, 32, 33), and modulation by GABA released from HCs (34, 35). These models are not necessarily mutually exclusive and unifying theories have been proposed (35, 36). Importantly, one of the central effects invariably observed in response to HC feedback is modulation of the $Ca_V1.4$ function at the active zones of cone terminals (32, 37). However, there is a significant void in our understanding of molecular mechanisms by which HCs modulate transmission of cone signals, mostly due to a paucity of players known to operate at this synapse. Identification and functional characterization of molecular elements involved in coordinating HC influence in cone synapses can transform our understanding of this enigmatic area of visual neuroscience.

Here, we performed an unbiased proteomic profiling of proteins selectively enriched in cone synapses. This led to identification of an adhesion G protein–coupled receptor (aGPCR), latrophilin3 (LPHN3), whose role in retina physiology, photoreceptor synaptic development, and function was previously unexplored. We show that alternative splicing of LPHN3 in the retina generates unique isoforms with distinct properties. Using mouse models, we demonstrate that changes in LPHN3 splicing regulate cone synaptic transmission transsynaptically by affecting $Ca_V1.4$ function. These findings reveal a molecular player with a pivotal role in regulating synaptic function of cone photoreceptors.

Results

Proteomic Profiling Identifies Cell-Adhesion Molecule LPHN3 to Be Associated with Cone Photoreceptors. Mammalian cone photoreceptors can be selectively labeled by peanut agglutinin (PNA), a lectin that recognizes a specific glycosylation pattern of cone proteins (38–40). We have confirmed cone selectivity of PNA labeling as well as prominent staining of cone synapses (Fig. 1*A*). A proteomic strategy was then devised to purify PNA-binding proteins followed by their mass-spectrometric identification to discover macromolecular complexes formed by cone-specific proteins with a focus on synapses (Fig. 1*B*). Mouse retinas were lysed, and the detergent extracts of membrane fraction were incubated with streptavidin beads in the presence or absence of biotinylated PNA. Proteins bound to the beads were eluted and subjected to mass-spectrometric identification (Fig. 1*B*). In total, we found 101 membrane proteins specifically purified only when PNA was present. Gene Ontology (GO) analysis indicated that 65 proteins are transmembrane and 28 proteins belong to glycoproteins, consistent with the nature of the PNA binding, with the rest presumably encompassing indirectly associated proteins within larger macromolecular complexes. Analysis using SynGO revealed 32 proteins with annotations related to synaptic formation and function (Fig. 1*C*). Ranking 11 proteins that satisfied all three filtering criteria identified synaptic cell-adhesion molecule (CAM) LPHN3 as the top hit with the highest unique peptides and spectral counts (Fig. 1*C*). LPHN3 is an aGPCR, featuring multiple extracellular domains known to interact with several synaptic partners as well as canonical 7-transmembrane (7-TM) bundle found in all GPCRs (Fig. 1*D*). We validated the identification of LPHN3 by incubating retina lysates with biotinylated PNA followed by pull-down with streptavidin beads. Western blot using anti-LPHN3 antibody detected the band only in the eluate of PNA-incubated sample, confirming that PNA was indeed able to pull-down LPHN3 (Fig. 1*E*).

To further validate the identification of LPHN3, we took advantage of the knock-in mouse model (41) containing an HA tag inserted in the extracellular portion of endogenous LPHN3 (LPHN3-HA KI) (*SI Appendix*, Fig. S1*A*). Western blotting with anti-HA antibodies detected the same band pattern that we observed using anti-LPHN3 antibody only in LPHN3-HA KI but not wild-type (WT) retinas (*SI Appendix*, Fig. S1*B*). Furthermore, the HA-reactive bands were specifically pulled down by the streptavidin beads only in the presence of biotinylated PNA (*SI Appendix*, Fig. S1*C*). In summary, our mass-spectrometric strategy identified LPHN3, a molecule not characterized in the retina previously, to be selectively associated with proteome of cone photoreceptors.

Transsynaptic Targeting of LPHN3 Expressed by HC to Cone Synapses. To study the localization of LPHN3 in the retina, we first performed immunohistochemistry (IHC) on retina cross-sections. Immunostaining revealed that LPHN3 is prominently present in the outer plexiform layer (OPL), a region where photoreceptor synapses are located (Fig. 2*A*). In the OPL, it showed a characteristic enrichment in islands reminiscent of cone pedicles. Indeed, costaining with cone arrestin revealed that LPHN3 is specifically localized at cone synapses (Fig. 2*B*). This localization of LPHN3 was further confirmed by in retinas from LPHN3-HA KI mice in which immunostaining with anti-HA antibody showed the same specific labeling pattern at the cone synapses (*SI Appendix*, Fig. S1 *D* and *E*).

The presence of LPHN3 in the synaptic cleft of cones may, in principle, be contributed by any one of the three types of neurons forming the tripartite synapse: photoreceptors, bipolar neurons, or HCs. To establish the identity of the neurons producing LPHN3, we examined cell-type specificity for its expression. In situ hybridization using a specific probe for *Adgrl3* messenger RNA (mRNA) encoding LPHN3 showed that the signal was absent from the photoreceptor layer but is most prominent in the OPL and the inner retina (Fig. 2*C*). The strong signal from the OPL suggested that LPHN3 may be preferentially expressed by HCs. Indeed, we confirmed the expression of LPHN3 in HCs by double in situ hybridization with a marker for HCs, calbindin (Fig. 2*D*). To further validate this observation, we analyzed previously published single-cell RNA-sequencing (RNA-seq) data (42, 43) and found that the majority of LPHN3 expression in the outer retina was mapped to the cellular population designated as HCs (*SI Appendix*, Fig. S2*A*). Finally, we performed immunohistochemical analysis staining LPHN3 together with two HC markers: calbindin and GABARρ2 (35). Both calbindin- and GABARρ2-labeled HC axon terminals and dendrites that synapse with rods and cones, respectively. We observed extensive colocalization of LPHN3 with GABARρ2 only at the HC dendrites that synapse with cones (Fig. 2*E* and *SI Appendix*, Fig. S2*B*), and this colocalization was further confirmed by high-power confocal imaging in combination with fluorescence intensity line-scan analysis (Fig. 2*F*). Together, these results establish LPHN3 as a synaptic molecule specifically localized at cone synapses but expressed by HCs.

Loss of LPHN3 in Mice Is Not Detrimental to Cone Synaptic Organization and Function. To begin studying the functional role of LPHN3 at the cone synapses, we first examined the effects of its complete ablation in mice. We used the null model in

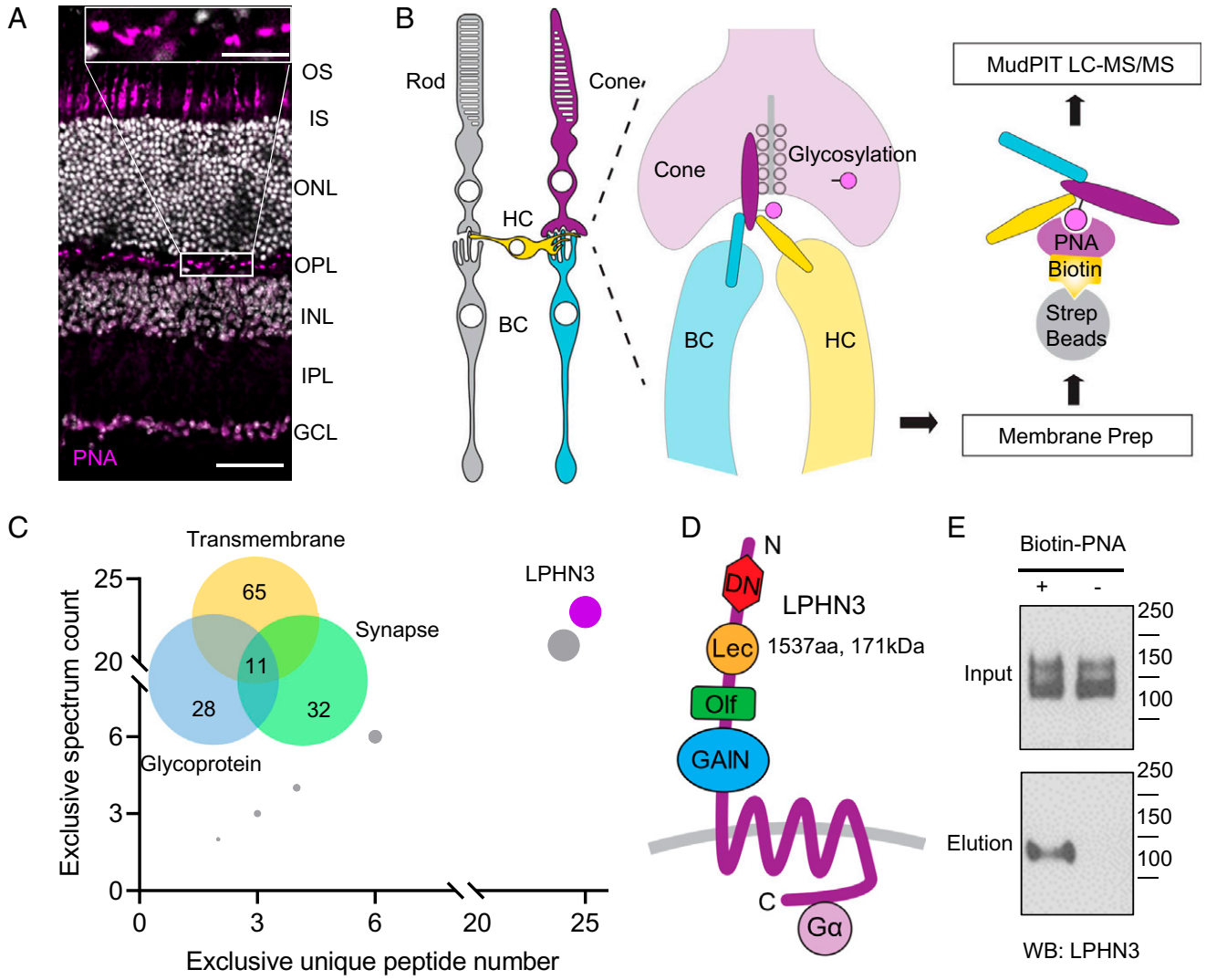

Fig. 1. Proteomic profiling identifies LPHN3 as a component of synaptic glycoproteome of cones. (*A*) Lectin PNA specifically labels cone photoreceptors. Mouse retina cross-sections were stained with Alexa Fluor 647–conjugated PNA revealing its localization at outer segment and synapse of cones. OS: outer segment, IS: inner segment, ONL: outer nuclear layer, INL: inner nuclear layer, IPL: inner plexiform layer, and GCL: ganglion cell layer (Scale bar, 50 μm). The insert shows the OPL at higher magnification (Scale bar, 10 μm). (*B*) Schematics of PNA pull-down purification and identification strategy of proteins specifically present in cone synapses. (*C*) Analysis of proteins specifically purified with PNA as identified by mass spectrometry. Venn diagram shows categorical classification of PNA enriched proteins by DAVID and SynGO Gene Ontology analysis. Rank order of the 11 proteins satisfying all three filter criteria shows that LPHN3 is the most abundant, highest-confidence candidate. (*D*) Domain composition of LPHN3. The protein contains extracellular DN, Lec, Olf, GPCR autoproteolysis inducing (GAIN) domains followed by the 7-TM and intracellular C terminus coupled with G protein. (*E*) PNA pull-down from WT retina lysate followed by Western blotting detecting with specific anti-LPHN3 antibody.

which *Adgrl3* gene is disrupted by introducing a gene trap after exon 10, which is predicted to prevent the translation of LPHN3 sequence early, essentially eliminating all its critical elements including the 7-TM region (44) (Fig. 3*A*). The resulting *Adgrl3* knockout (KO) mice were bred to homozygosity and consistent with prediction, their retinas completely lacked expression of LPHN3 when analyzed by Western blotting (Fig. 3*B*). This was paralleled by loss of LPHN3 immunostaining in all synaptic layers (Fig. 3*C*). We found that overall morphology of the KO retinas to be normal with no signs of retina degeneration until at least 10 mo of age (*SI Appendix*, Fig. S3 *A*–*C*).

We then studied the impact of LPHN3 loss on synaptic cytoarchitechture of cones. Immunostaining for the presynaptic ribbon organizer CTBP2 and the postsynaptic glutamate receptor mGluR6 on the dendritic tips of ON-BCs followed by the quantification on their mean fluorescence intensity within cone pedicles showed no significant changes between the genotypes (Fig. 3 *D* and *E*). We next assessed functional impact of LPHN3 loss by evaluating cone synaptic transmission to ON-BC using electroretinography (ERG). We first probed cone transmission in dark-adapted state using photopic flashes, which activate both rod and cone photoreceptors. Once activated, photoreceptors hyperpolarize and generate an electrically negative a-wave, and as the signal is transmitted across the synapse, rod and cone ON-BCs depolarize producing the positive b-waves (Fig. 3*F*). The bright flashes produced robust a-waves with amplitude and kinetics indistinguishable between the genotypes (*SI Appendix*, Fig. S3 *D* and *E*), suggesting the normal phototransduction in both rod and cone photoreceptors. Surprisingly, we found that neither amplitude nor implicit time of the b-wave were significantly affected in the KO mice (Fig. 3 *F* and *H* and *SI Appendix*, Fig. S3*F*). To more specifically

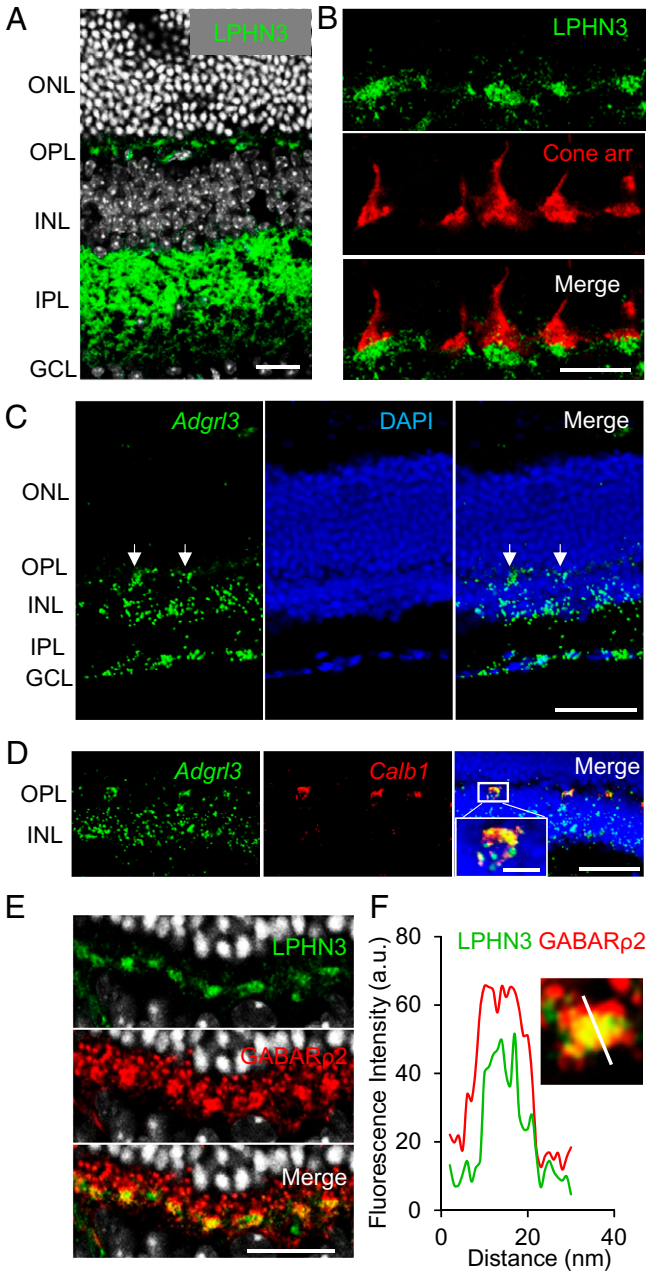

Fig. 2. LPHN3 is specifically targeted to cone synapse and expressed by HCs. (*A*) Immunohistochemical detection of LPHN3 by staining retina cross-sections with anti-LPHN3 antibody. The signal is enriched synaptically at both outer and inner plexiform layers (Scale bar, 20 μm). (*B*) LPHN3 is specifically targeted at cone synapse as revealed by colabeling with cone marker, cone arrestin (Scale bar, 10 μm). (*C*) Cell specificity of LPHN3 expression revealed by in situ hybridization for *Adgrl3* mRNA (Scale bar, 50 μm). Strong fluorescence signal is detected in the OPL (white arrows). (*D*) Double in situ hybridization for *Adgrl3* mRNA (green) and HC specific *Calb1* (calbindin) mRNA (red) revealed HC origin of *Adgrl3* expression at OPL. (*E*) Selective expression of LPHN3 at the dendrites of HCs. Mouse retina cross-sections were costained with LPHN3 and HC synaptic marker, GABA receptor ρ2 subunit (GABARρ2) (Scale bar, 20 μm). (*F*) Analysis of LPHN3 localization in synaptic puncta relative to GABARρ2 by coimmunostaining of retina cross-section with the indicated antibodies. The insert shows fluorescence quantification of LPHN3 distribution across synaptic puncta relative to GABARρ2 determined by scanning fluorescence intensity along the white line.

evaluate the transmission in the cone pathway, we performed light-adapted ERG in which rod-saturating background light was applied to isolate cone-driven response. Analysis showed comparable a-wave amplitudes between WT and KO, confirming the normal phototransduction in cones of KO mice (*SI Appendix*, Fig. S3*G*). Again, analysis of the b-wave amplitudes across the range of the eliciting flash intensities showed no significant differences between KO animals and their WT littermates (Fig. 3 *G* and *I*). Together, these results indicate that loss of LPHN3 does not significantly affect cone photoreceptor synaptic structure and function.

LPHN3 in the Retina Is Alternatively Spliced Generating an Abundant Isoform Lacking Exon 5. The lack of observable phenotype upon complete elimination of LPHN3 prompted us to examine its splicing patterns in the retina, as synaptic CAMs are known to be heavily diversified by alternative splicing which critically shapes their function (45). In fact, evidence suggests that splice isoforms could behave more like distinct proteins than minor variants of the same protein (46), indicating the need to diversify genetic strategies beyond global null models to fully unveil the function of a gene. Using long-read capture sequencing (47), we identified over 400 distinct *Adgrl3* mRNA isoforms expressed in mouse retina. Much of this diversity arises due to extensive alternative splicing occurring in both the extra- and intracellular regions of LPHN3 (Fig. 4*A* and *SI Appendix*, Fig. S4*A*). Reasoning that extracellular domains of LPHN3 are major determinants of its synaptic properties, we focused on examining its splicing within the extracellular portion in detail. Interestingly, distribution of exons in this portion of the gene largely mapped to identified domains in the encoded protein (Fig. 4*B*). Analysis on the exon usage in the extracellular region revealed that multiple exons are alternatively spliced to a varying degree with exon 5 being the most frequently affected by splicing followed by exon 8 and exon 14 (Fig. 4*C*). To determine whether splicing events were coordinated, we performed an exon usage correlation analysis on all 422 full-length mRNAs contained within our LPHN3 isoform catalog (*SI Appendix*, Fig. S4*B*). Among the three most spliced extracellular exons, there appears to be a potential long-range coupling between exon 8 and exon 14 as evidenced by a Pearson Correlation coefficient of 0.6 (Fig. 4*D*). In contrast, exon 5 does not reveal strong coupling to other exons including exon 8 and exon 14 (Fig. 4*D* and *SI Appendix*, Fig. S4*B*), suggesting an independent nature of the alternative splicing at exon 5. To determine whether the alternative splicing of LPHN3 generates different protein products, we immunoblotted retina lysates using an anti-LPHN3 antibody and detected two major bands migrating close to each other (Fig. 4*E*). After calibrating the band mobilities against molecular weight ladders, the calculated difference in size between the two bands matched the expected shift caused by the loss of exon 5 of ~6 to 7 kDa (Fig. 4*E*). To exclude possible interference from posttranslational modification of LPHN3 by glycosylation on band mobility, retina lysates were subjected to deglycosylation, which increased the mobility of both bands but maintained the same difference in size (*SI Appendix*, Fig. S4*C*). Exon 5 encodes the very distal N terminus of LPHN3 that we designate as DN. It comprises 68 amino acids located immediately after the predicted signal peptide and right before lectin-like (Lec) domain (Fig. 4*B*). A variant lacking exon 5 is predicted to generate a LPHN3 protein preserving all known extracellular domains but missing the DN domain (Fig. 4*F*). Together, our findings reveal that LPHN3 in the retina is alternatively spliced, and we identified a previously unknown abundant splice isoform lacking exon 5 (LPHN3ΔE5) expressed at a level comparable to that of the full-length protein.

The DN Domain Encoded by Exon 5 Regulates Association of LPHN3 with Its Synaptic Binding Partners. LPHN3 is thought to regulate synaptic function via interaction with its partners teneurins

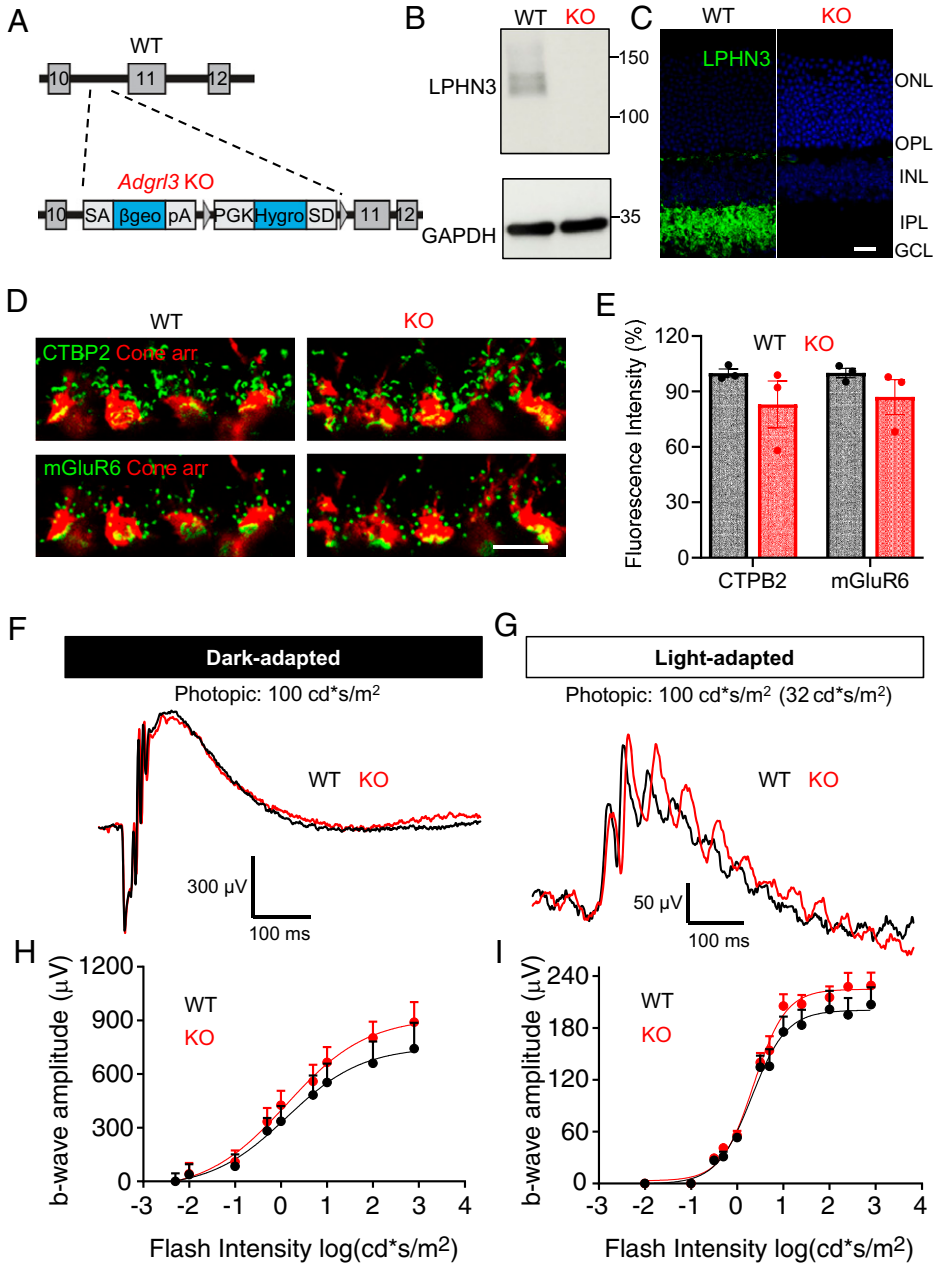

Fig. 3. Loss of LPHN3 in mice does not perturb cone synaptic organization and function. (*A*) Schematic of the strategy for disrupting *Adgrl3* expression in mice. A gene trap vector containing a promoter trap module (SAβgeo*pA) and a poly-A trap module (PGKhygSD) (83) was introduced in the intron10 of *Adgrl3*. (*B*) Elimination of LPHN3 expression shown by Western blotting using anti-LPHN3 antibody. (*C*) Elimination of LPHN3 staining revealed by immunostaining retina cross sections with anti-LPHN3 antibody (Scale bar, 20 μm). (*D*) Representative images of WT and KO retina cross sections immunostained with antibodies as indicated. (Scale bar, 10 μm.) (*E*) Quantification of mean fluorescence intensity of CTBP2 and mGluR6 at the cone synapse of WT and KO retinas. The data were averaged from three mice of each genotype. Error bars are SEM values and unpaired Student's *t* test. (*F*) Representative dark-adapted ERG traces from WT and KO mice stimulated with photopic light at 100 cd*s/m^2. (*G*) Representative light-adapted (32 cd*s/m^2) ERG traces from WT and KO mice stimulated with photopic light at 100 cd*s/m^2. (*H*) Stimulus intensity–response curves of dark-adapted ERG b-wave amplitude plotted against flash intensity in the photopic range. Six animals for each genotype. Error bars are SEM values and multiple Student's *t* test. (*I*) Stimulus intensity–response curve of light-adapted (32 cd*s/m^2) ERG b-wave amplitude plotted against flash intensity in the photopic range. Seven mice for WT and six mice for KO. Error bars are SEM values and multiple Student's *t* test.

(TENs) and fibronectin leucine–rich transmembrane (FLRT) proteins (41, 48, 49). Our structural modeling based on the previously reported structure (50–52) suggests that the DN domain is located within molecular interaction distance with both TEN2 and FLRT3 (*SI Appendix*, Fig. S5*A*). Importantly, in situ hybridization assay revealed that both *Tenm2* and *Flrt3* are expressed by cone photoreceptors (Fig. 5*A*). Immunolabeling of TEN2 and FLRT3 on retina sections showed that both proteins are located in the synaptic cleft at cone synapses (Fig. 5*B*). Thus, we set out to determine the influence of the DN domain on these interactions using two strategies. First, we reconstituted cells with representative LPHN3 binding partners TEN2 or FLRT3 and probed their ability to associate with purified recombinant ectodomains of LPHN3 either with (FL) or without (ΔDN) DN sequence using flow cytometry (Fig. 5*C*). Using this strategy, we found that both FL and ΔDN protein

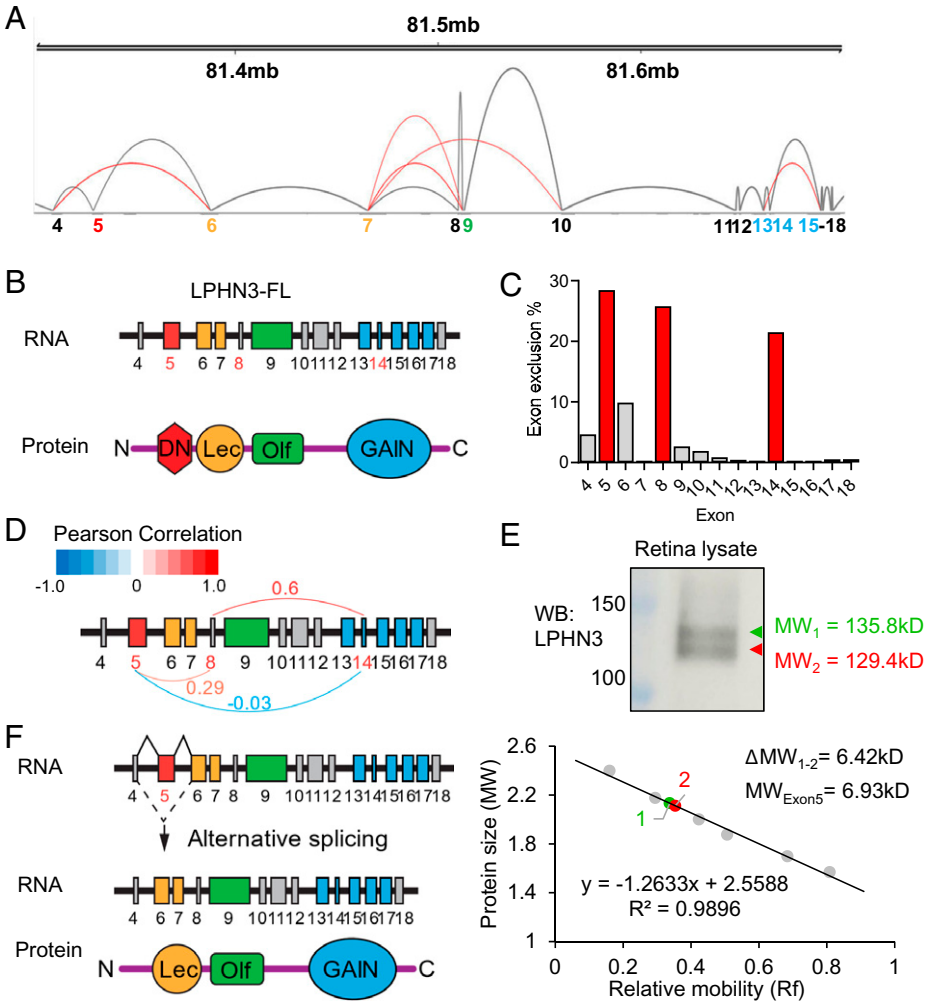

Fig. 4. Alternative splicing map of LPHN3 in the retina. (*A*) Sashimi plot generated from long-read RNA sequencing data demonstrating alternative splicing within the extracellular exons (4–18) of *Adgrl3* gene together with genomic coordinates on the top and exon numbers at the bottom color-coded according to the domains they encode. Gray arcs connect neighboring exons representing canonical splicing, and red arcs connect nonneighboring exons representing alternative splicing. (*B*) Schematic of LPHN3 mRNA and corresponding domains of the protein in the extracellular region. Each domain is coded in the same color as its corresponding exon(s). (*C*) Bar graph showing the exclusion rate of exons encoding LPHN3 ectodomains. (*D*) Pearson correlation analysis on the most alternatively spliced exons (5, 8, 14). The coefficient value ranges from −1.0 to 1.0 with −1.0 being completely inversely correlated and 1.0 being completely positively correlated. Analysis shows a potential coordinated splicing event between exon 8 and 14 (coefficient value = 0.6) but low correlation in coordinated splicing between exon 5 and the other two exons (coefficient of 0.29 and −0.03). (*E*) Two major isoforms of LPHN3, LPHN3 full-length (LPHN3 FL), and LPHN3 lacking exon5 (LPHN3ΔE5), are expressed in WT retina. (*Top*) Western blotting of WT retina lysate using specific anti-LPHN3 antibody. (*Bottom*) Standard curve of relative mobility values of protein ladders plotted against the corresponding log values of their molecular weight (MW). The difference in the MW between the two isoforms (6.42 kD) matches with the predicted MW of the region encoded by exon 5 (6.93 kD). (*F*) Schematic of alternative splicing at exon 5 leading to generation of LPHN3ΔE5 isoform lacking the DN region.

robustly bound to cells expressing TEN2 and FLRT3 in a dose-dependent manner (Fig. 5*D* and *SI Appendix*, Fig. S5*B*). Importantly, ΔDN exhibited significantly greater binding as compared to FL protein at lower concentrations with both interaction partners. This difference was no longer observed as interaction reached saturation suggesting that removal of DN domain increased binding affinity of LPHN3 for both TEN2 and FLRT3 (Fig. 5 *D* and *E*).

Our second strategy relied on pull-down assays between purified Fc-tagged ectodomains of LPHN3 immobilized on the beads and either TEN2 or FLRT3 expressed in cells and released by lysis in detergent (Fig. 5 *F* and *H*). Again, we observed robust binding of both FL and ΔDN proteins to TEN2 and FLRT3 (Fig. 5 *G* and *I*). Quantification revealed an approximately twofold increase in binding efficiency of ΔDN with TEN2 as compared to FL (Fig. 5*J*) in agreement with the flow cytometry results. We did not detect significant differences between FL and ΔDN binding to FLRT3 likely due to saturating conditions of the pull-down assay for this higher-affinity binding (Fig. 5*J*). Since the interaction between LPHNs and other isoforms of TENs and FLRTs have also been previously reported (53), we next asked whether other TENs and FLRTs are expressed by photoreceptors and whether the effect of DN on LPHN3 interaction is conserved across other isoforms. We first characterized the expression profile of all *Flrts* and *Tenms* in the retina using in situ hybridization and found that most *Flrt* and *Tenm* isoforms are indeed expressed by photoreceptors (*SI Appendix*, Fig. S5 *C–G*). We then tested the binding of the same FL and ΔDN protein with TEN and FLRT isoforms. Similar to the results of TEN2 and FLRT3, we observed robust binding of both LPHN3 proteins to all the other TEN and FLRT isoforms tested (*SI Appendix*, Fig. S5 *C–G*). Interestingly, we found that the binding efficiency of ΔDN with TEN1 is significantly increased compared to that of FL (*SI Appendix*, Fig. S5*E*) and that the binding efficiency with TEN3 and TEN4 shows a trend of increase which did not reach statistical significance (*SI Appendix*, Fig. S5 *F* and *G*). In contrast, for several FLRT isoforms, we found no significant differences in the binding between FL and ΔDN (*SI Appendix*, Fig. S5 *C* and *D*). This systematic characterization of LPHN3 binding to different TENs and FLRTs suggests that the modulatory effect of DN region on LPHN3 interactions is isoform specific. Together, these observations indicate that HC-expressed LPHN3 is engaged in transsynaptic interactions with multiple binding partners and that the DN domain encoded by exon 5 inhibits the heterophilic interactions of LPHN3 such that LPHN3 lacking exon 5 sequence likely generates a gain-of-function variant with an augmented engagement of transsynaptic binding partners.

Specific Disruption of Alternative Splicing at Exon 5 of LHPN3 Impairs Cone Synaptic Function. To investigate the physiological role of splice isoform LPHN3ΔE5, we evaluated a mouse model in which exon 5 of *Adgrl3* was selectively eliminated leaving other elements in place (ΔE5). The replacement of exon 5

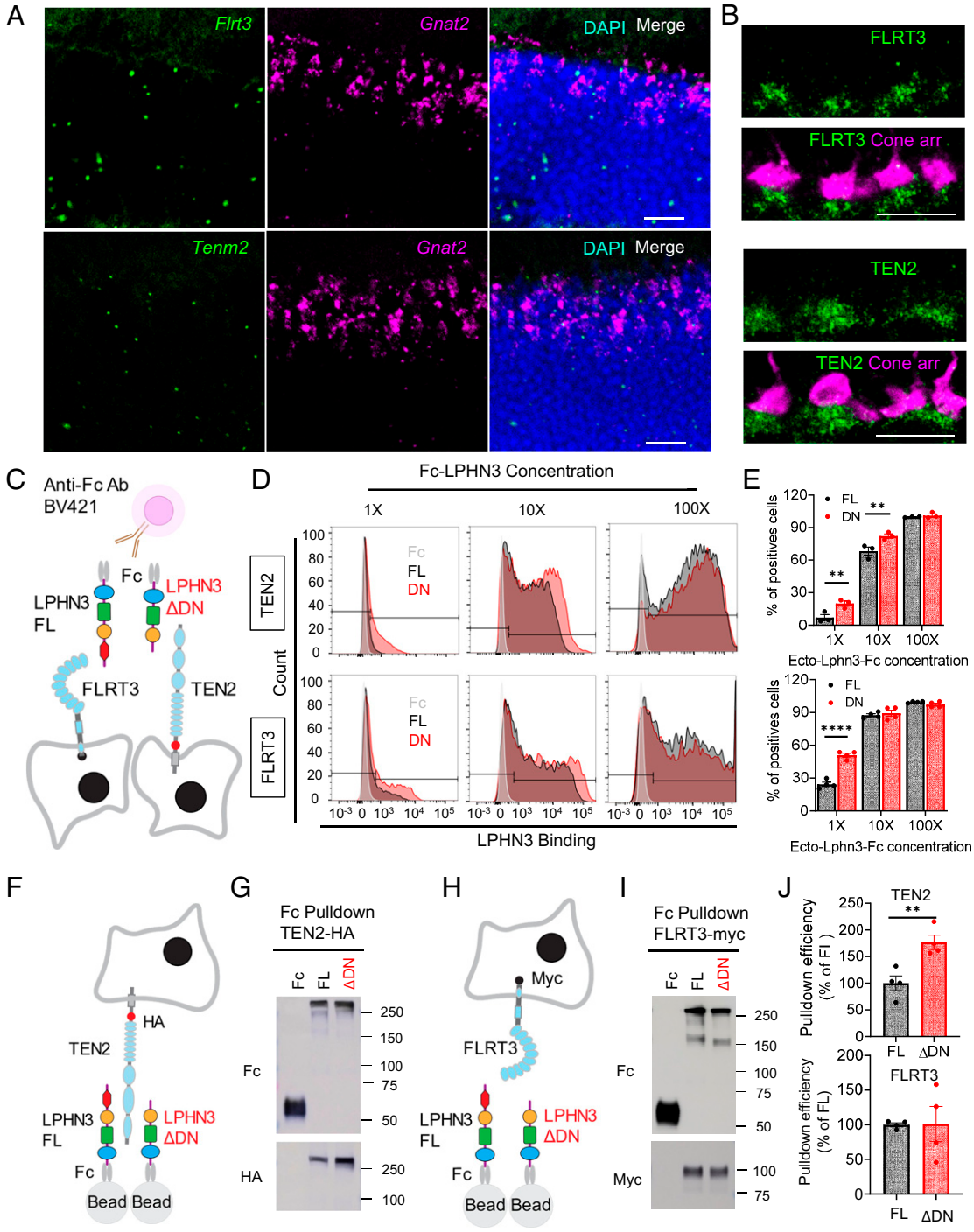

Fig. 5. Deletion of DN domain of LPHN3 encoded by exon 5 alters interactions with CAMs. (*A*) Expression profile of LPHN3 binders, TEN2 and FLRT3, revealed by in situ hybridization for *Tenm2* and *Flrt3* mRNA (Scale bar, 20 μm). Fluorescence signal (green) is detected in the ONL. Double in situ hybridization with cone-specific *Gnat2* (cone transducin) mRNA (purple) revealed a cone origin of *Tenm2* and *Flrt3* expression. (*B*) Synaptic targeting of FLRT3 and TEN2 at the cone synapses. Mouse retina cross-sections were costained with cone arrestin (purple) and FLRT3 (green, *Top*) or TEN2 (green, *Bottom*) antibodies (Scale bar, 10 μm). (*C*) Schematic of flow cytometry used for studying LPHN3-mediated protein–protein interactions. Fc-tagged ecto domain of full-length (FL) and the alternatively spliced isoform without exon5 (ΔDN) were incubated with HEK cells transfected with either FLRT3 or TEN2 followed by incubation with detection fluorescent anti-Fc antibody. (*D*) Representative flow cytometry histograms showing LPHN3 isoforms binding to TEN2 (top) and FLRT3 (bottom) in a dose-dependent manner. Fc only (control) and an equivalent amount of Fc-tagged FL and ΔDN LPHN3 proteins with different dilutions were incubated with the same batch of transfected cells expressing either TEN2 or FLRT3. (*E*) Quantification of the flow cytometry experiments described in *D*. The percentages of positively transfected cells bound with LPHN3 FL or ΔDN proteins were calculated to reflect binding affinity of LPHN3 isoforms toward different binding partners. Error bars are SEM values. For TEN2, $n = 3$ and $^{**}P < 0.01$, and for FLRT3, $n = 4$, $^{****}P < 0.0001$, and unpaired *t* test. (*F*) Schematic of the pull-down assay for studying LPHN3 isoforms interacting with TEN2. (*G*) Representative Western blotting result of Fc only (control) and Fc-tagged LPHN3 isoforms interacting with HA-tagged TEN2. (*H*) Schematic of the pull-down assay for studying LPHN3 isoforms interacting with FLRT3. (*I*) Representative Western blotting result of Fc only (control) and Fc-tagged LPHN3 isoforms interacting with Myc-tagged FLRT3. (*J*) Quantification of the pull-down assay described in *G* and *I*. Pull-down TEN2 (*Top*) or FLRT3 (*Bottom*) signal was normalized to LPHN3 protein pull-down signal to get the pull-down efficiency. Error bars are SEM values. $n = 4$, $^{**}P < 0.01$, and unpaired Student's *t* test.

by the LacZ/Neo cassette is predicted to specifically exclude exon 5 from being integrated into the final protein (Fig. 6*A*). To confirm the intended modification, we performed RT-PCR amplifying the region containing exon 5 for both WT and ΔE5 retina. Gel electrophoresis revealed two bands from WT retina sample, with the top one at 2.1 kb and the bottom at 1.9 kb, matching the predicted size of the FL and ΔE5 transcript, respectively. Unlike WT, only the 1.9-kb band was detected in ΔE5 retina (Fig. 6*B*), suggesting the successful skipping of exon 5 at the mRNA level. To further confirm this modification at the protein level, we performed Western blotting and found that only the lower band representing LPHN3ΔE5 isoform was detected in ΔE5 mice (Fig. 6*C*).

We next studied the impact of eliminating exon 5 of *Adgrl3* on synaptic formation and function of cone photoreceptors. Immunostaining revealed no significant change in LPHN3 synaptic targeting in ΔE5 mice, confirming the normal expression and trafficking of LPHN3ΔE5 isoform (Fig. 6 *D* and *E*). Immunostaining for presynaptic marker CTBP2 and the postsynaptic marker mGluR6 showed no apparent changes in ΔE5 retina. Quantification of the mean fluorescent intensity of CTBP2 and mGluR6 staining within cone synapse confirmed the normal targeting of these key synaptic molecules in ΔE5 retina (Fig. 6 *D* and *E*). To assess the functional impact of eliminating exon 5, we first performed dark-adapted ERG stimulating with photopic flashes. Robust a-waves with comparable amplitude and implicit time were generated in both WT and ΔE5 mice, suggesting the normal phototransduction in ΔE5 mice (*SI Appendix*, Fig. S6 *A* and *B*). Analysis of the ERG b-wave across the same intensity range revealed that neither amplitude nor implicit time were affected in ΔE5 mice (Fig. 6 *F* and *H* and *SI Appendix*, Fig. S6*C*). Strikingly, when rod-saturating background was applied, we observed a substantial reduction in b-wave amplitude across nearly all photopic flash intensities in ΔE5 mice as compared to WT littermates (Fig. 6 *G* and *I*). In contrast, the a-wave remained unchanged (*SI Appendix*, Fig. S6*D*), suggesting that cone to ON-CBC synaptic transmission is impaired in ΔE5 mice. To confirm the altered synaptic function

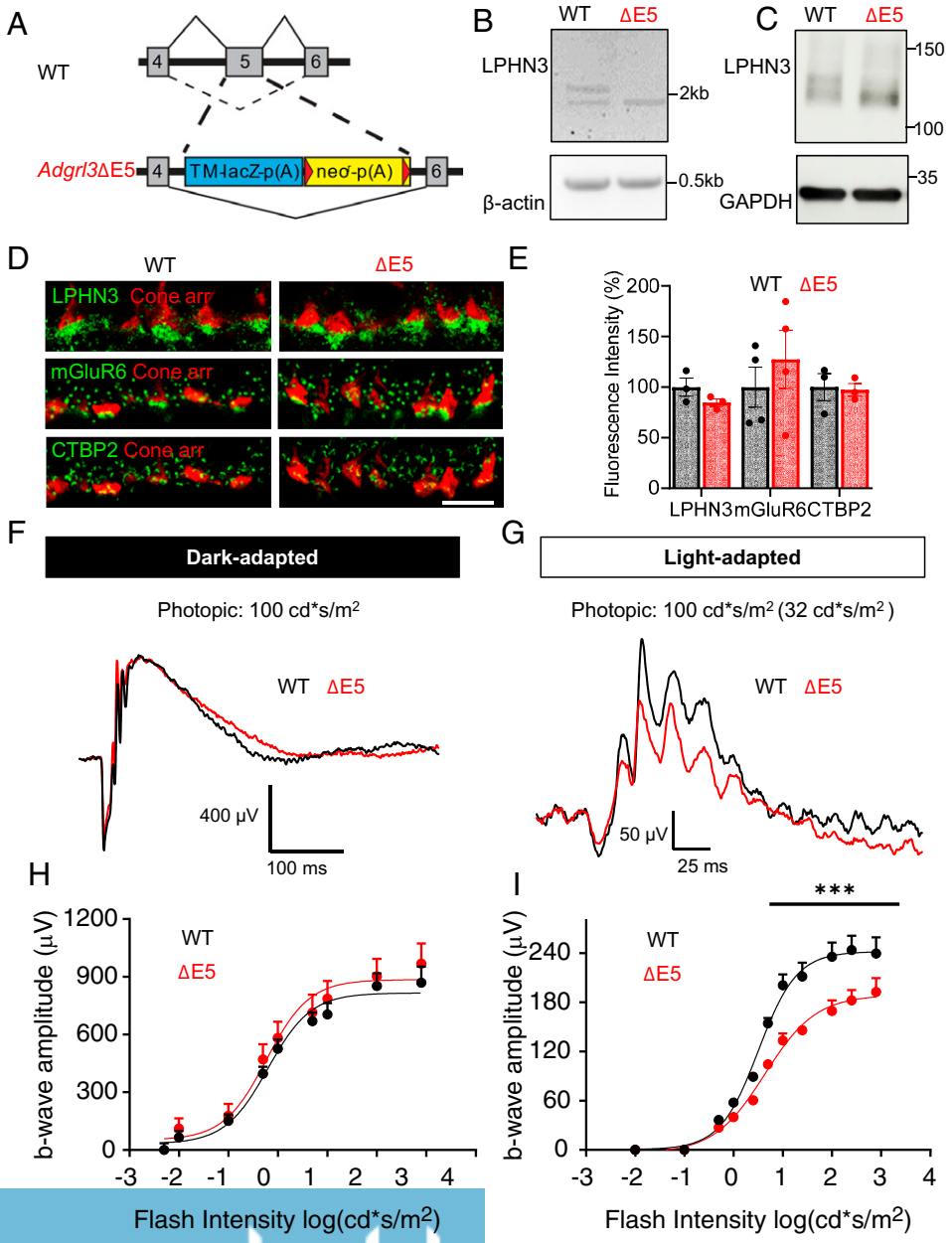

Fig. 6. Specific disruption of splicing at exon5 of *Adgrl3* impairs cone synaptic function. (*A*) Schematic of the strategy for disrupting splicing at exon 5 of *Adgrl3* in mice. (*B*) Specific elimination of exon 5-containing transcripts of *Adgrl3* in ΔE5 retina shown by RT-PCR. β-actin was used as loading control. (*C*) Specific elimination of exon5 containing LPHN3 isoforms expressed in ΔE5 retina shown by Western blotting using anti-LPHN3 antibody. GAPDH was used as loading control. (*D*) Representative images of WT and ΔE5 retina cross sections immunostained with antibodies as indicated. (Scale bar, 10 μm.) (*E*) Quantification of mean fluorescence intensity of LPHN3, CTBP2, and mGluR6 at the cone synapse of WT and ΔE5 retinas. The data were averaged from three to four mice of each genotype. Error bars are SEM values and unpaired Student's *t* test. (*F*) Representative dark-adapted ERG traces from WT and ΔE5 mice stimulated with photopic light at 100cd*s/m^2. (*G*) Representative light-adapted (32 cd*s/m^2) ERG traces from WT and ΔE5 mice stimulated with photopic light at 100 cd*s/m^2. (*H*) Stimulus intensity–response curve of dark-adapted ERG b-wave amplitude plotted against flash intensity in the photopic range. Six animals for WT and seven for ΔE5 were used. Error bars are SEM values and multiple Student's *t* test. (*I*) Stimulus intensity–response curve of light-adapted (32 cd*s/m^2) ERG b-wave amplitude plotted against flash intensity in the photopic range. Four mice for WT and five mice for ΔE5 were used. Error bars are SEM values, ***$P < 0.001$, and multiple Student's *t* test.

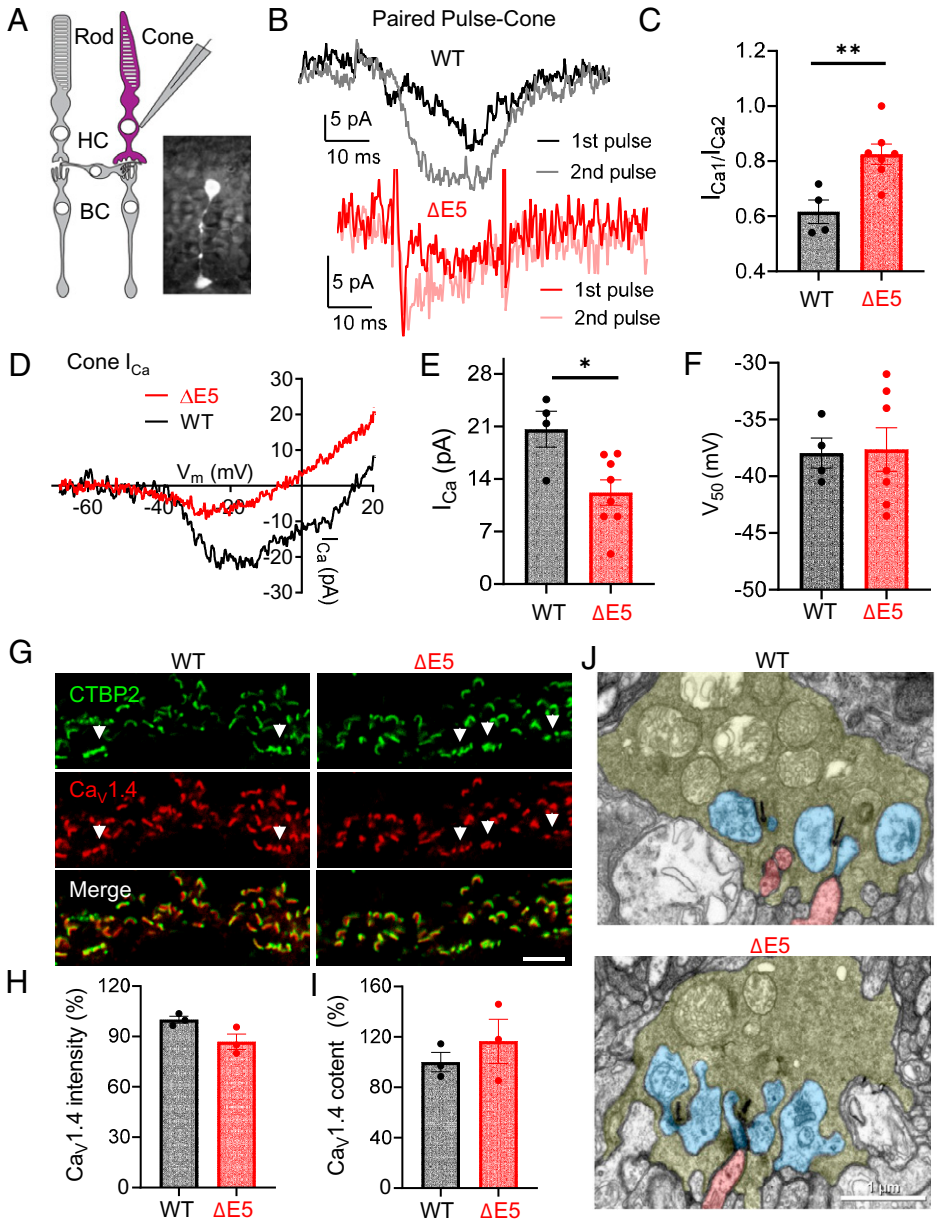

Fig. 7. LPHN3ΔE5 variant reduces cone synaptic release and inhibits calcium channel function. (*A*) Schematic of retinal slice recording from cone photoreceptors. The inset shows a cone filled with sulfarhodamine B in WT retinal slice. (*B*) Representative traces documenting paired-pulse inhibition of I_{Ca} in a control WT cone (*Top*). Application of a depolarizing test step (25 ms, −70 to −10 mV) evoked a transient inward current followed by a brief outward current deflection reflecting inhibition by vesicular protons. Due to the depletion of releasable vesicles by the first pulse, this proton-mediated inhibition was abolished during the second pulse applied 50 ms later. (*Bottom*) Representative traces documented showing limited paired-pulse inhibition of I_{Ca} in a ΔE5 cone. (*C*) Quantification of the paired-pulse ratio (amplitude of I_{Ca} evoked by the first pulse/amplitude of I_{Ca} evoked by the second pulse) between control WT (n = 4) and ΔE5 (n = 7) cones (**P < 0.01, unpaired Student's t test, and error bars are SEM values). The larger paired-pulse ratio in ΔE5 cones indicates that less glutamate was released in these cones. (*D*) Representative traces of I_{Ca} from ΔE5 (red trace) and control WT cones (black trace) evoked by a ramp voltage protocol (−102.5 to +47.5 mV, 0.5 mV/ms). (*E*) I_{Ca} peak amplitude measured with ramp voltage protocols was reduced significantly in ΔE5 cones (red, n = 8; *P < 0.05, unpaired Student's t test, and error bars are SEM values) relative to control WT cones (n = 4). (*F*) Analysis of the midpoint of activation voltage of calcium channels in cones of WT (n = 4) and ΔE5 (n = 7) retinas. Data are shown as mean ± SEM, unpaired Student's t test. (*G*) Representative images of WT and ΔE5 retina sections immunostained with antibodies indicated (Scale bar, 5 μm). (*H*) Quantification of the mean fluorescence intensity of $Ca_V1.4$ at cone synapse of WT (black, n = 3) and ΔE5 (red, n = 3) retinas. Error bars are SEM values and unpaired Student's t test. (*I*) Quantification of the area occupied by $Ca_V1.4$ at cone synapse of WT (black, n = 3) and ΔE5 (red, n = 3) retinas. Error bars are SEM values and unpaired Student's t test. (*J*) Analysis on the ultrastructure of cone synapse of WT and ΔE5 retina by EM. Cone terminals are labeled in pale green, HC processes in blue, and bipolar dendrites in red (Scale bar, 1 μm).

is specific for cones, we also examined the rod synaptic transmission in ΔE5 retina and found comparable scotopic b-wave amplitude and implicit time to those of WT retina (*SI Appendix*, Fig. S6 *C* and *E*). Together, these findings revealed a critical role of LPHN3 in regulating cone synaptic function and that this regulation involved the DN region of the molecule encoded by exon 5 of *Adgrl3*.

LPHN3ΔE5 Variant Inhibits Vesicular Release of Cones by Inhibiting Ca^{2+} Channel Function. To determine the mechanisms of the effects on the cone synaptic transmission observed in ΔE5 mice, we focused on the presynaptic neurotransmitter release machinery for the known role of HC in modulating this process in cones (32, 37) (Fig. 7*A*). To probe for changes in synaptic release, we analyzed the inhibition of I_{Ca} produced by protons that are coreleased with glutamate during fusion of synaptic vesicles. Release of vesicular protons from cones causes a transient inhibition of presynaptic cone I_{Ca} (54–56) during exocytosis. Brief depolarizing steps were used to activate inward I_{Ca} in WT and ΔE5 cones. Proton-mediated inhibition of I_{Ca} in rods and cones was often sufficiently rapid to obscure the initial inward portion of I_{Ca}, yielding a slowly developing inward current as proton-mediated inhibition diminished during the test step (Fig. 7*B*). To show that the source of protons was exocytosis of low-pH vesicular contents, we used a paired-pulse protocol to deplete the pool of available synaptic vesicles (57–59). In this protocol, a second 25-ms test pulse was applied 50 ms after the end of a first 25-ms pulse, causing marked presynaptic depression in photoreceptors. We measured the amount of inhibition by comparing the amplitude of I_{Ca} evoked during the first step (I_{Ca1}) with that evoked by the second step (I_{Ca2}). Proton-mediated inhibition on I_{Ca} was reduced from 38.4 ± 4.3% in control cones to 17.5 ± 3.7% in ΔE5 cones (Fig. 7*C*). Although activation kinetics of cone I_{Ca} during 25-ms voltage steps were often obscured by rapid proton-mediated inhibition, the time constants for activation (τ_{on}) and

de-activation (τ_{off}) did not appear to differ (τ_{on}, control, 2.69 ± 1.27 ms; τ_{on} ΔE5, 2.28 ± 1.12 ms; control τ_{off}, 4.76 ± 0.51 ms; and ΔE5 τ_{off} 3.69 ± 0.58 ms) (*SI Appendix*, Fig. S7 *A* and *B*). To test whether this reduction in I_{Ca} was specific for cones, we also performed the same recordings from rods (*SI Appendix*, Fig. S7*C*). I_{Ca} is smaller in rods but also showed paired-pulse inhibition of I_{Ca} (*SI Appendix*, Fig. S7*D*). Unlike cones, paired-pulse inhibition of rod I_{Ca} was not significantly reduced in ΔE5 mice (*SI Appendix*, Fig. S7*E*).

The release of glutamate from cone pedicles is controlled by the voltage-gated Ca^{2+} channel $Ca_v1.4$ clustered beneath synaptic ribbons (60–62). Thus, we next evaluated changes in Ca^{2+} currents (I_{Ca}) mediated by $Ca_V1.4$ as possible underlying mechanism by applying a ramp voltage protocol (Fig. 7*D*). Comparison of the current/voltage relationship between WT and ΔE5 cones revealed that the peak amplitude of I_{Ca} attained during the ramp protocol was reduced significantly in ΔE5 cones compared to that of WT (Fig. 7*E*). The midpoint activation voltage (V_{50}), however, was not altered significantly (Fig. 7*F*). Unlike cones, neither the amplitude nor V_{50} of I_{Ca} in rods was significantly changed in ΔE5 mice as compared to controls (*SI Appendix*, Fig. S7 *F–H*).

To test whether the reduced Ca^{2+} current is due to diminished $Ca_V1.4$ content at cone synapse, we performed IHC analysis on $Ca_V1.4$ in WT and ΔE5 retina section. Quantification on both the mean fluorescence intensity and the total size of $Ca_V1.4$ in cones showed no significant difference between genotypes (Fig. 7 *G–I*), suggesting that the reduced I_{Ca} in ΔE5 cones is not due to a lower amount of $Ca_V1.4$ targeted to the cone synapse but rather due to diminished channel activity. Finally, our electron microscopy (EM) studies showed that the ultrastructure of cone synapses was also intact in ΔE5 retinas, as reflected by normal ribbon, HC processes, and invagination from cone ON-CBs (Fig. 7*J*). Together, these results demonstrate that LPHN3 plays an important role in regulating $Ca_V1.4$ activity and synaptic release in cone photoreceptors via a mechanism involving the action of the DN region of LPHN3.

Discussion

Modulation of neurotransmitter release is central for visual information encoding by the cone photoreceptors (22, 63). The key role in this process belongs to HCs that have powerful effects on synaptic transmission at the cone synapse (23). However, the molecular mechanisms underlying HC-mediated modulation of cone synaptic release are not well defined due to a paucity in identification and functional characterization of critical molecular players involved in this process. The main advance of this study is the discovery that an adhesion GPCR, LPHN3, plays critical role in modulation of cone synaptic transmission by HC. We established that LPHN3 acts transsynaptically in HCs to affect the activity of calcium channels in cone terminals. In the process of investigating the mechanism of this modulation, we discovered that this LPHN3-dependent function involves a molecular element (DN domain) of the receptor encoded by exon 5, which is regulated by alternative splicing (Fig. 8). Based on our observations, we propose a model in which the DN domain modulates the interaction of LPHN3 with its transsynaptic partners, which in turn control the activity of the calcium channel to regulate synaptic release at the cone synapse (Fig. 8).

LPHN isoforms are emerging as key regulators of synapse formation and function in brain (41, 48, 49, 52, 64). However, their roles in the ribbon synapse of the sensory systems have never been studied. We found that LPHN3 expression in the mouse retina is specifically enriched at synapses in both outer and inner retina. Moreover, we found that LPHN3 is selectively localized at cone but not rod synapses. This specificity results

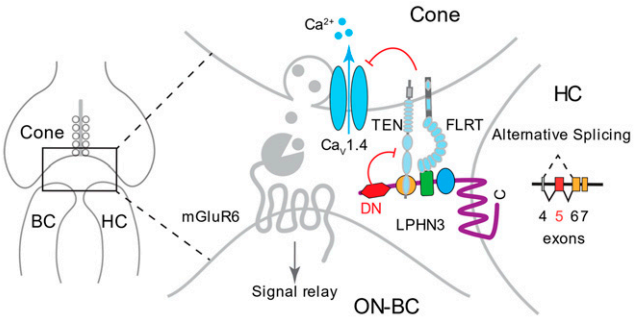

Fig. 8. Schematic of proposed role of LPHN3 in modulating cone synaptic transmission. LPHN3 is selectively expressed by HCs and targeted to the cone synapse. LPHN3 regulates cone synaptic release, possibly through transsynaptic interaction with TENs and FLRTs at the synapse, which in turn inhibit the activity of calcium channel $Ca_V1.4$. Alternative splicing at exon 5 of *Adgrl3* generates LPHN3ΔE5 isoform lacking the DN region, which increases LPHN3 association with TENs and FLRTs inhibiting $Ca_V1.4$ function.

from the selective localization of LPHN3 at dendrites but not axons of HCs. This differential subcellular targeting of LPHN3 in HCs is reminiscent of the selective localization of LPHN3 to the dendritic domains in CA1 pyramidal neurons (41), supporting the idea that LPHN3 plays a critical role in directing synapse specificity throughout the central nervous system (CNS).

The finding that neither the structure nor the function of cone synapse is overtly affected upon LPHN3 deletion is surprising given that LPHN3 loss of function was sufficient to affect synapse formation and function in hippocampal neurons (41, 49). One possible explanation could be compensation by other LPHNs, which share >50% sequence identity with LPHN3. Both LPHN1 and LPHN2 have been shown playing critical roles in synapse formation and function (64, 65). In fact, LPHN2 and LPHN3 were found to be functionally redundant in synaptic function of cerebellar Purkinje cell (66). Thus, a similar situation with redundant involvement of several LPHN isoforms may also play out in retinal synapses. Our study argues that unlike loss of function, augmentation of LPHN function has a greater impact resulting in readily detectable effects on synaptic transmission. Thus, enhancing LPHN function, which can be achieved in part by the mobilization of specific variants and isoforms, may be used to adjust synaptic properties. Interestingly, the functional effects associated with enhanced LPHN3 function were not encumbered by structural alterations in either number or size of synaptic contacts, commonly observed in LPHN3 loss-of-function models (41, 49, 66), further arguing for the unique nature of LPHN3 regulatory mechanisms. Collectively, our findings suggest that LPHN3 is essential for enabling the proper functional specification but not the physical establishment of cone synapses and that LPHN3 utilizes distinct yet overlapping mechanism to instruct synapse specialization at different synapses.

How does LPHN3 regulate cone synaptic function? Our whole-cell recording data show that modulating presynaptic calcium channel activity is one major mechanism. This is in line with the well-established role of HCs in regulating cone calcium channels through the extensively studied feedback mechanism (24). Despite ongoing debate about the molecular determinants responsible for the feedback mechanism, emerging consensus indicates that modulation of calcium channel activity by HCs plays a major role in shaping synaptic output of cones (67). We propose that LPHN3 regulates $Ca_V1.4$ function and neurotransmitter release in a transsynaptic manner by influencing the network of cell adhesion complexes that tie to the presynaptic release apparatus of cones. One characteristic feature of HC

feedback inhibition is the change in both amplitude and voltage dependence of the calcium current (I_{Ca}) (32, 37). Interestingly, recordings of cone I_{Ca} from our ΔE5 model revealed drastic reduction only in amplitude but not in voltage dependence. This selective effect of LPHN3 on amplitude is unique and further supports a hypothesis regarding the transsynaptic nature of $Ca_V1.4$ modulation via a distinct mechanism different from previously reported canonical feedback regulation. Several types of CAMs, including FLRTs and TENs, have been identified as binding partners of LPHN3 (48, 49, 51, 68, 69). Although in general, CAMs like TENs and FLRTs have been implicated in retinal circuit formation and function (70–72), their role in photoreceptors or in shaping calcium channel activity or synaptic transmission has not been reported. Both our in situ hybridization results and previously published single-cell RNA-seq study (73) show that most isoforms of TENs and FLRTs are expressed in photoreceptors of the mouse retina. Moreover, we find LPHN3 and its binding partners to be present at cone synapses. Together with changes in binding that we observe, our data suggest a mechanism whereby LPHN3 transsynaptically regulates presynaptic calcium channel complex to affect synaptic transmission. Determining the exact mechanisms of the identified transsynaptic regulation of $Ca_V1.4$ complex at cone synapses and the contribution of individual TEN and FLRT isoforms will be an exciting future direction.

Alternative splicing of CAMs has been emerging as a powerful program to instruct the synapse specification (74). Interestingly, different splicing isoforms of LPHNs have been shown to display distinct functions in nonneuronal cells (75–77). Despite the critical role of LPHN3 in synapse formation and function, how alternative splicing regulates endogenous LPHN3 function in CNS has not been reported. One of the major insights presented in this study stems from systematic investigation of alternative splicing of LPHN3 that led to the identification of a splice isoform lacking exon 5 with major effects on LPHN3 function. We confirmed an abundant expression of LPHN3ΔE5 isoform at the protein level and found it to be the most frequent modification of LPHN3 involving the extracellular portion of the receptor. By using a mouse model with isoform-selective ablation of LPHN3, we were able to provide in vivo evidence of the physiological relevance of alternative splicing of LPHNs.

Our results also provide insights into the regulation of LPHN3 interaction with synaptic CAMs. We identified an element upstream from previously characterized structural domains that we call DN domain and demonstrated that this DN domain regulates binding of LPHN3 to TENs and FLRTs. Our structural modeling suggests that the inhibitory effect of the DN domain is likely explained by the steric hindrance that it imposes on the association of TENs and FLRTs which occurs at a nearby Lec and Olfectomedin-like (Olf) domains, respectively (51, 52, 78, 79). The DN splicing isoform is distinct from a previously reported SSA variant in LPHN1, which was shown to inhibit interaction of that LPHN family member with TEN2 and TEN4 but not FLRT3 (77). This alternatively spliced SSA sequence is encoded by exon 8, which is wedged between Lec and Olf domains. The different effects of DN and SSA on LPHN's interaction with synaptic CAMs suggest that these elements induce distinct conformational changes in the LPHN to differentially influence interactions with its partners. Collectively, studies on LPHNs' alternative splicing suggest that distinct LPHN isoforms with unique binding profiles may contribute to shaping synaptic specificity (80). Fine-tuning the expression balance of isoforms may also allow neurons to adjust their responses according to changing external stimuli.

Finally, our findings have implications outside of the visual system. Clinically, several independent genetic studies linked polymorphisms in *ADGRL3* with attention deficit hyperactivity disorder (ADHD) susceptibility (81). At least two ADHD-associated single nucleotide polymorphisms have been mapped to splice sites within the introns and predicted to cause abnormal splicing (82). Our findings argue that alteration in alternative splicing leads to prominent changes in LPHN3 interactions and synaptic function. Thus, we speculate that ADHD susceptibility may be contributed, at least partly, by aberrant LPHN3 function caused by the imbalanced expression profile of various LPHN3 isoforms. Whether and how alternative splicing of LPHN3 is temporally and spatially regulated and how the spatiotemporal regulation plays a role in diversifying LPHN3 function remain an important and exciting future direction.

Materials and Methods

Procedures involving mice strictly followed NIH guidelines and were approved by the Institutional Animal Care and Use Committees at Scripps Florida and the University of Nebraska. Methods performed in the current study involved generation of cDNA constructs, cell culture, flow cytometry, mass spectrometry, long-read RNA sequencing, immunoprecipitation, in situ hybridization, IHC, ERG, single-cell patch clamp recordings, structural modeling, and EM. Extensive details pertaining to these techniques are available in *SI Appendix*.

Data Availability. All study data are included in the article and/or *SI Appendix*.

ACKNOWLEDGMENTS. We thank Ms. Natalia Martemyanova for producing and maintaining mice examined in this study. We thank Light Microscopy Core in Max Planck Florida Institute for Neuroscience for supporting image acquisition. We thank Dr. Demet Araç (University of Chicago) for the gift of TEN2 construct and Dr. Klaus-Peter Lesch for facilitating sharing of Lphn3 KO mouse strain. This work was supported by NIH Grants EY030554 (Y.W.), EY018139 (K.A.M.), EY10542 (W.B.T.), EY024694 (J.N.K.), EY031445 (J.N.K.), EY026344 (T.A.R.), and EY5722 (Duke University). This work is also supported by Research to Prevent Blindness (unrestricted grant to Duke University).

1. R. H. Masland, The neuronal organization of the retina. *Neuron* **76**, 266–280 (2012).
2. M. Hoon, H. Okawa, L. Della Santina, R. O. Wong, Functional architecture of the retina: Development and disease. *Prog. Retin. Eye Res.* **42**, 44–84 (2014).
3. M. E. Burns, V. Y. Arshavsky, Beyond counting photons: Trials and trends in vertebrate visual transduction. *Neuron* **48**, 387–401 (2005).
4. N. T. Ingram, A. P. Sampath, G. L. Fain, Why are rods more sensitive than cones? *J. Physiol.* **594**, 5415–5426 (2016).
5. T. D. Lamb, Why rods and cones? *Eye (Lond.)* **30**, 179–185 (2016).
6. D. A. Burkhardt, Light adaptation and photopigment bleaching in cone photoreceptors in situ in the retina of the turtle. *J. Neurosci.* **14**, 1091–1105 (1994).
7. K. W. Yau, R. C. Hardie, Phototransduction motifs and variations. *Cell* **139**, 246–264 (2009).
8. J. I. Korenbrot, Speed, adaptation, and stability of the response to light in cone photoreceptors: The functional role of Ca-dependent modulation of ligand sensitivity in cGMP-gated ion channels. *J. Gen. Physiol.* **139**, 31–56 (2012).
9. J. F. Ashmore, D. R. Copenhagen, An analysis of transmission from cones to hyperpolarizing bipolar cells in the retina of the turtle. *J. Physiol.* **340**, 569–597 (1983).
10. F. Mansergh *et al.*, Mutation of the calcium channel gene Cacna1f disrupts calcium signaling, synaptic transmission and cellular organization in mouse retina. *Hum. Mol. Genet.* **14**, 3035–3046 (2005).
11. N. T. Bech-Hansen *et al.*, Loss-of-function mutations in a calcium-channel alpha1-subunit gene in Xp11.23 cause incomplete X-linked congenital stationary night blindness. *Nat. Genet.* **19**, 264–267 (1998).
12. T. M. Strom *et al.*, An L-type calcium-channel gene mutated in incomplete X-linked congenital stationary night blindness. *Nat. Genet.* **19**, 260–263 (1998).
13. T. M. Bartoletti *et al.*, Release from the cone ribbon synapse under bright light conditions can be controlled by the opening of only a few Ca(2+) channels. *J. Neurophysiol.* **106**, 2922–2935 (2011).
14. W. B. Thoreson, K. Rabl, E. Townes-Anderson, R. Heidelberger, A highly Ca2+-sensitive pool of vesicles contributes to linearity at the rod photoreceptor ribbon synapse. *Neuron* **42**, 595–605 (2004).
15. T. Pangrsic, J. H. Singer, A. Koschak, Voltage-gated calcium channels: Key players in sensory coding in the retina and the inner ear. *Physiol. Rev.* **98**, 2063–2096 (2018).
16. F. Haeseleer *et al.*, Essential role of Ca2+-binding protein 4, a Cav1.4 channel regulator, in photoreceptor synaptic function. *Nat. Neurosci.* **7**, 1079–1087 (2004).
17. C. P. Grabner *et al.*, RIM1/2-mediated facilitation of Cav1.4 channel opening is required for Ca2+-stimulated release in mouse rod photoreceptors. *J. Neurosci.* **35**, 13133–13147 (2015).

18. Y. Wang *et al.*, The auxiliary calcium channel subunit α2δ4 is required for axonal elaboration, synaptic transmission, and wiring of rod photoreceptors. *Neuron* **93**, 1359–1374.e6 (2017).
19. S. H. DeVries, D. A. Baylor, Synaptic circuitry of the retina and olfactory bulb. *Cell* **72** (suppl.), 139–149 (1993).
20. S. Haverkamp, U. Grünert, H. Wässle, The cone pedicle, a complex synapse in the retina. *Neuron* **27**, 85–95 (2000).
21. S. H. DeVries, W. Li, S. Saszik, Parallel processing in two transmitter microenvironments at the cone photoreceptor synapse. *Neuron* **50**, 735–748 (2006).
22. S. L. Jackman *et al.*, Role of the synaptic ribbon in transmitting the cone light response. *Nat. Neurosci.* **12**, 303–310 (2009).
23. C. A. Chapot, T. Euler, T. Schubert, How do horizontal cells 'talk' to cone photoreceptors? Different levels of complexity at the cone-horizontal cell synapse. *J. Physiol.* **595**, 5495–5506 (2017).
24. W. B. Thoreson, S. C. Mangel, Lateral interactions in the outer retina. *Prog. Retin. Eye Res.* **31**, 407–441 (2012).
25. D. A. Baylor, M. G. Fuortes, P. M. O'Bryan, Lateral interaction between vertebrate photoreceptors. *Vision Res.* **11**, 1195–1196 (1971).
26. C. A. Chapot *et al.*, Local signals in mouse horizontal cell dendrites. *Curr. Biol.* **27**, 3603–3615.e5 (2017).
27. S. L. Jackman, N. Babai, J. J. Chambers, W. B. Thoreson, R. H. Kramer, A positive feedback synapse from retinal horizontal cells to cone photoreceptors. *PLoS Biol.* **9**, e1001057 (2011).
28. B. Beckwith-Cohen, L. C. Holzhausen, T. M. Wang, R. Rajappa, R. H. Kramer, Localizing proton-mediated inhibitory feedback at the retinal horizontal cell-cone synapse with genetically-encoded pH probes. *J. Neurosci.* **39**, 651–662 (2019).
29. J. J. Grassmeyer, W. B. Thoreson, Synaptic ribbon active zones in cone photoreceptors operate independently from one another. *Front. Cell. Neurosci.* **11**, 198 (2017).
30. A. L. Byzov, T. M. Shura-Bura, Electrical feedback mechanism in the processing of signals in the outer plexiform layer of the retina. *Vision Res.* **26**, 33–44 (1986).
31. M. Kamermans *et al.*, Hemichannel-mediated inhibition in the outer retina. *Science* **292**, 1178–1180 (2001).
32. L. Cadetti, W. B. Thoreson, Feedback effects of horizontal cell membrane potential on cone calcium currents studied with simultaneous recordings. *J. Neurophysiol.* **95**, 1992–1995 (2006).
33. H. Hirasawa, A. Kaneko, pH changes in the invaginating synaptic cleft mediate feedback from horizontal cells to cone photoreceptors by modulating Ca2+ channels. *J. Gen. Physiol.* **122**, 657–671 (2003).
34. S. M. Wu, Input-output relations of the feedback synapse between horizontal cells and cones in the tiger salamander retina. *J. Neurophysiol.* **65**, 1197–1206 (1991).
35. J. C. R. Grove *et al.*, Novel hybrid action of GABA mediates inhibitory feedback in the mammalian retina. *PLoS Biol.* **17**, e3000200 (2019).
36. R. Vroman *et al.*, Extracellular ATP hydrolysis inhibits synaptic transmission by increasing ph buffering in the synaptic cleft. *PLoS Biol.* **12**, e1001864 (2014).
37. J. Verweij, M. Kamermans, H. Spekreijse, Horizontal cells feed back to cones by shifting the cone calcium-current activation range. *Vision Res.* **36**, 3943–3953 (1996).
38. J. C. Blanks, L. V. Johnson, Specific binding of peanut lectin to a class of retinal photoreceptor cells. A species comparison. *Invest. Ophthalmol. Vis. Sci.* **25**, 546–557 (1984).
39. K. Kawano, F. Uehara, M. Sameshima, N. Ohba, Binding sites of peanut agglutinin in mammalian retina. *Jpn. J. Ophthalmol.* **28**, 205–214 (1984).
40. K. Unoki, F. Uehara, M. Sameshima, K. Nakano, N. Ohba, Specific binding of peanut agglutinin to foveal and peripheral cone photoreceptors of monkey retina. *Ophthalmic Res.* **20**, 112–116 (1988).
41. R. Sando, X. Jiang, T. C. Südhof, Latrophilin GPCRs direct synapse specificity by coincident binding of FLRTs and teneurins. *Science* **363**, eaav7969 (2019).
42. M. Menon *et al.*, Single-cell transcriptomic atlas of the human retina identifies cell types associated with age-related macular degeneration. *Nat. Commun.* **10**, 4902 (2019).
43. B. S. Clark *et al.*, Single-cell RNA-seq analysis of retinal development identifies NFI factors as regulating mitotic exit and late-born cell specification. *Neuron* **102**, 1111–1126.e5 (2019).
44. D. Wallis *et al.*, Initial characterization of mice null for Lphn3, a gene implicated in ADHD and addiction. *Brain Res.* **1463**, 85–92 (2012).
45. B. Raj, B. J. Blencowe, Alternative splicing in the mammalian nervous system: Recent insights into mechanisms and functional roles. *Neuron* **87**, 14–27 (2015).
46. X. Yang *et al.*, Widespread expansion of protein interaction capabilities by alternative splicing. *Cell* **164**, 805–817 (2016).
47. T. A. Ray *et al.*, Comprehensive identification of mRNA isoforms reveals the diversity of neural cell-surface molecules with roles in retinal development and disease. *Nat. Commun.* **11**, 3328 (2020).
48. J. Li *et al.*, Structural basis for teneurin function in circuit-wiring: A toxin motif at the synapse. *Cell* **173**, 735–748.e15 (2018).
49. M. L. O'Sullivan *et al.*, FLRT proteins are endogenous latrophilin ligands and regulate excitatory synapse development. *Neuron* **73**, 903–910 (2012).
50. Y. C. Lu *et al.*, Structural basis of latrophilin-FLRT-UNC5 interaction in cell adhesion. *Structure* **23**, 1678–1691 (2015).
51. J. Li *et al.*, Alternative splicing controls teneurin-latrophilin interaction and synapse specificity by a shape-shifting mechanism. *Nat. Commun.* **11**, 2140 (2020).
52. D. Del Toro *et al.*, Structural basis of teneurin-latrophilin interaction in repulsive guidance of migrating neurons. *Cell* **180**, 323–339.e19 (2020).
53. A. L. Moreno-Salinas *et al.*, Latrophilins: A neuro-centric view of an evolutionary conserved adhesion G protein-coupled receptor subfamily. *Front. Neurosci.* **13**, 700 (2019).
54. S. H. DeVries, Exocytosed protons feedback to suppress the Ca2+ current in mammalian cone photoreceptors. *Neuron* **32**, 1107–1117 (2001).
55. M. J. Palmer, C. Hull, J. Vigh, H. von Gersdorff, Synaptic cleft acidification and modulation of short-term depression by exocytosed protons in retinal bipolar cells. *J. Neurosci.* **23**, 11332–11341 (2003).
56. P. F. Y. Vincent *et al.*, Clustered Ca^{2+} channels are blocked by synaptic vesicle proton release at mammalian auditory ribbon synapses. *Cell Rep.* **25**, 3451–3464.e3 (2018).
57. K. Rabl, L. Cadetti, W. B. Thoreson, Paired-pulse depression at photoreceptor synapses. *J. Neurosci.* **26**, 2555–2563 (2006).
58. C. P. Grabner, C. P. Ratliff, A. C. Light, S. H. DeVries, Mechanism of high-frequency signaling at a depressing ribbon synapse. *Neuron* **91**, 133–145 (2016).
59. B. Innocenti, R. Heidelberger, Mechanisms contributing to tonic release at the cone photoreceptor ribbon synapse. *J. Neurophysiol.* **99**, 25–36 (2008).
60. C. W. Morgans, Localization of the alpha(1F) calcium channel subunit in the rat retina. *Invest. Ophthalmol. Vis. Sci.* **42**, 2414–2418 (2001).
61. C. Lv, T. J. Gould, J. Bewersdorf, D. Zenisek, High-resolution optical imaging of zebrafish larval ribbon synapse protein RIBEYE, RIM2, and CaV 1.4 by stimulation emission depletion microscopy. *Microsc. Microanal.* **18**, 745–752 (2012).
62. A. Lee *et al.*, Characterization of Cav1.4 complexes (α11.4, β2, and α2δ4) in HEK293T cells and in the retina. *J. Biol. Chem.* **290**, 1505–1521 (2015).
63. S. Y. Choi *et al.*, Encoding light intensity by the cone photoreceptor synapse. *Neuron* **48**, 555–562 (2005).
64. G. R. Anderson *et al.*, Postsynaptic adhesion GPCR latrophilin-2 mediates target recognition in entorhinal-hippocampal synapse assembly. *J. Cell Biol.* **216**, 3831–3846 (2017).
65. N. V. Vysokov *et al.*, Proteolytically released Lasso/teneurin-2 induces axonal attraction by interacting with latrophilin-1 on axonal growth cones. *eLife* **7**, e37935 (2018).
66. R. S. Zhang, K. Liakath-Ali, T. C. Südhof, Latrophilin-2 and latrophilin-3 are redundantly essential for parallel-fiber synapse function in cerebellum. *eLife* **9**, e54443 (2020).
67. R. H. Kramer, C. M. Davenport, Lateral inhibition in the vertebrate retina: The case of the missing neurotransmitter. *PLoS Biol.* **13**, e1002322 (2015).
68. A. A. Boucard, J. Ko, T. C. Südhof, High affinity neurexin binding to cell adhesion G-protein-coupled receptor CIRL1/latrophilin-1 produces an intercellular adhesion complex. *J. Biol. Chem.* **287**, 9399–9413 (2012).
69. V. A. Jackson *et al.*, Super-complexes of adhesion GPCRs and neural guidance receptors. *Nat. Commun.* **7**, 11184 (2016).
70. A. Cheung, K. E. Trevers, M. Reyes-Corral, P. Antinucci, R. Hindges, Expression and roles of teneurins in zebrafish. *Front. Neurosci.* **13**, 158 (2019).
71. J. J. Visser *et al.*, An extracellular biochemical screen reveals that FLRTs and Unc5s mediate neuronal subtype recognition in the retina. *eLife* **4**, e08149 (2015).
72. P. Antinucci, N. Nikolaou, M. P. Meyer, R. Hindges, Teneurin-3 specifies morphological and functional connectivity of retinal ganglion cells in the vertebrate visual system. *Cell Rep.* **5**, 582–592 (2013).
73. S. Sarin *et al.*, Role for Wnt signaling in retinal neuropil development: Analysis via RNA-seq and in vivo somatic CRISPR mutagenesis. *Neuron* **98**, 109–126.e8 (2018).
74. E. Furlanis, P. Scheiffele, Regulation of neuronal differentiation, function, and plasticity by alternative splicing. *Annu. Rev. Cell Dev. Biol.* **34**, 451–469 (2018).
75. J. Rothe *et al.*, Involvement of the adhesion GPCRs latrophilins in the regulation of insulin release. *Cell Rep.* **26**, 1573–1584.e5 (2019).
76. J. C. Ovando-Zambrano, J. A. Arias-Montaño, A. A. Boucard, Alternative splicing event modifying ADGRL1/latrophilin-1 cytoplasmic tail promotes both opposing and dual cAMP signaling pathways. *Ann. N. Y. Acad. Sci.* **1456**, 168–185 (2019).
77. A. A. Boucard, S. Maxeiner, T. C. Südhof, Latrophilins function as heterophilic cell-adhesion molecules by binding to teneurins: Regulation by alternative splicing. *J. Biol. Chem.* **289**, 387–402 (2014).
78. F. M. Ranaivoson *et al.*, Structural and mechanistic insights into the latrophilin3-FLRT3 complex that mediates glutamatergic synapse development. *Structure* **23**, 1665–1677 (2015).
79. V. A. Jackson *et al.*, Structural basis of latrophilin-FLRT interaction. *Structure* **23**, 774–781 (2015).
80. B. Honig, L. Shapiro, Adhesion protein structure, molecular affinities, and principles of cell-cell recognition. *Cell* **181**, 520–535 (2020).
81. E. M. Bruxel *et al.*, Meta-analysis and systematic review of ADGRL3 (LPHN3) polymorphisms in ADHD susceptibility. *Mol. Psychiatry.***26**, 2277–2285 (2020).
82. M. Arcos-Burgos *et al.*, A common variant of the latrophilin 3 gene, LPHN3, confers susceptibility to ADHD and predicts effectiveness of stimulant medication. *Mol. Psychiatry* **15**, 1053–1066 (2010).
83. W. V. Chen, J. Delrow, P. D. Corrin, J. P. Frazier, P. Soriano, Identification and validation of PDGF transcriptional targets by microarray-coupled gene-trap mutagenesis. *Nat. Genet.* **36**, 304–312 (2004).